

Related self-similar statistics of the turbulent/non-turbulent interface and the turbulence dissipation

Y. Zhou and J.C. Vassilicos

Turbulence, Mixing and Flow Control Group,
Department of Aeronautics, Imperial College London
London, SW7 2AZ, United Kingdom

(Received ?; revised ?; accepted ?. - To be entered by editorial office)

The scalings of the local entrainment velocity v_n of the turbulent/non-turbulent interface and of the turbulence dissipation rate are closely related to each other in an axisymmetric and self-similar turbulent wake. The turbulence dissipation scaling implied by the Kolmogorov equilibrium cascade phenomenology is consistent with a Kolmogorov scaling of v_n whereas the non-equilibrium dissipation scaling reported for various turbulent flows in Vassilicos (2015), Dairay *et al.* (2015), Goto & Vassilicos (2016a) and Obligado *et al.* (2016) is consistent with a different scaling of v_n . We present results from a DNS of a spatially developing axisymmetric and self-similar turbulent wake which supports this conclusion and the assumptions that it is based on.

1. Introduction

The study of the turbulent/non-turbulent (TNT) interface starts with the seminal work of Corrsin & Kistler (1955) who studied it in a boundary layer, a plane wake and a circular jet. In defining this interface they recognised that vorticity is a defining characteristic of fluid turbulence so that the interface separates vortical from potential flow. They also understood that the non-vortical fluid can only become turbulent by viscous diffusion of vorticity from the vortical side of the interface and they identified the laminar superlayer as part of the inner structure of the thin TNT interface. Another part of this inner structure was identified about fifty years later because of the advent of Direct Numerical Simulations (DNS) and Particle Image Velocimetry, a sort of buffer layer between the fully turbulent region of the flow and the viscous superlayer which is sometimes referred to as turbulent sublayer (see da Silva *et al.* (2014)).

Corrsin & Kistler (1955) argued that the thickness of the viscous superlayer scales with the Kolmogorov length-scale η_K of the turbulence. The DNS study by Taveira & da Silva (2014) supported this scaling for shear-free turbulence and planar turbulent jets. Whilst, with the exception of shear-free turbulence, the thickness of the TNT interface generally seems to be close to the Taylor microscale (see da Silva *et al.* (2014)), recent DNS of turbulent mixing layers (Watanabe *et al.* (2015)) and turbulent wakes (Watanabe *et al.* (2016)) report that the thickness of the interface scales with η_K . Given that the viscous superlayer spreads by viscous processes, its local propagation velocity is proportional to η_K divided by the viscous time η_K^2/ν and therefore scales as the Kolmogorov velocity $u_\eta \sim \nu/\eta_K$ where ν is the kinematic viscosity of the fluid. This scaling of the local propagation velocity, the local entrainment velocity, has been confirmed in oscillating grid turbulence by Holzner & Lüthi (2011) both experimentally and computationally and in the DNS of a turbulent mixing layer by Watanabe *et al.* (2015).

Corrsin & Kistler (1955) also studied the statistics of the location of the TNT interface and suggested that these statistics scale with the length-scale characterising the mean velocity profile, for example the wake or jet width in the case of a turbulent wake or jet. LaRue & Libby (1976) obtained some experimental evidence for such a scaling by comparing two streamwise positions in a planar wake. One might indeed expect that the way the TNT interface fluctuates and spreads with downstream distance in a wake or jet does indeed have a critical influence on the way the wake/jet mean width grows with streamwise distance.

A parallel line of enquiry and analysis which goes back to Townsend (1976) has now established (Townsend (1976), George (1989), Nedić *et al.* (2013), Dairay *et al.* (2015), Obligado *et al.* (2016)) that the wake/jet width's dependence on streamwise distance is intimately related to the turbulence dissipation scalings in self-preserving turbulent free shear flows. There must therefore be a comparably intimate relation between the scalings of the turbulent/non-turbulent interface and those of the turbulence dissipation, at least in self-similar turbulent shear flows. In this paper, which is concerned with the particular case of the axisymmetric and self-similar turbulent wake, we develop this point and argue that the turbulence dissipation scalings are closely related to the scalings of the local thickness and local entrainment velocity in ways which lead to some non-trivial conclusions.

Some basic theoretical considerations concerning the relation between turbulence dissipation scalings and the scalings of the local propagation velocity of the TNT interface are developed in section 2. In section 3 we use DNS to assess the assumptions and results of section 2 and we conclude with a discussion and a summary of our main results in section 4.

2. What is the relation between the local entrainment velocity and the turbulence dissipation?

One might think that the answer to this question is well known and simple and consists in saying that the local entrainment velocity scales as ν/η_I as per Corrsin & Kistler (1955) where the interface thickness η_I is a length-scale, such as for example the Kolmogorov microscale $\eta_K \sim (\nu^3/\epsilon)^{1/4}$, which depends on the turbulence dissipation rate ϵ . In this section we argue that this answer is too simplistic, if not strictly speaking wrong in general, and we develop a more detailed and complete answer to the question.

It is both rare to find and difficult to obtain fully resolved spatio-temporal 3D data of a turbulent flow. It can also be cumbersome and time-consuming to store and analyse such data. We therefore develop methods of analysis which can be applied to 2D planar cuts through the flow, specifically planes orthogonal to the axis of rotational symmetry of an axisymmetric turbulent flow. In this paper we apply our methods to the self-similar axisymmetric turbulent wake.

We start by defining a characteristic local entrainment velocity v_n , i.e. characteristic local propagation velocity of the TNT interface, in terms of the time-averaged area A of the fully turbulent region in a plane normal to the axis of symmetry of the flow and the time-averaged length \mathcal{L} of the TNT interface in the same plane. This axis of symmetry is aligned with the streamwise direction and coincides with the centreline for the flow. At a streamwise distance x from the wake generator, the rate of change of $A = A(x)$ is given by the integral of the local propagation velocity of the TNT interface over the entire length of the interface. We can express this integral as $\mathcal{L}v_n$ where the characteristic local entrainment velocity v_n is in fact an average local propagation velocity in a sense defined exactly in the Appendix. As the rate of change of $A = A(x)$ can be approximated by

$U_\infty dA/dx$ far enough from the wake generator, we write

$$U_\infty \frac{dA}{dx} = \mathcal{L}v_n \quad (2.1)$$

where U_∞ is the freestream velocity. This equation is derived in the Appendix from first principles, namely incompressibility and the motion of iso-lines.

The instantaneous radial distance R_I of the TNT interface from the centreline is a function of streamwise distance x , azimuthal angle ϕ around the centreline and time t and is defined in a 2D plane normal to the centreline. At a distance x from the wake generator where the turbulent wake is statistically axisymmetric around the centreline, the probability density function (pdf) of R_I is independent of ϕ and only a function of x . To determine this pdf $P(R_I; x)$ one can collect statistics over time and ϕ in a 2D plane and test whether this pdf scales with the wake width $\delta(x)$, as first suggested by the intermittency results of Corrsin & Kistler (1955) and as one might expect in the self-similar region of the turbulence wake, i.e. whether $P(R_I; x) = \delta^{-1}p(R_I/\delta)$. Such a pdf of R_I would suggest[†] that $A(x) \sim \delta^2(x)$ allowing us to determine the scalings of v_n from

$$U_\infty \delta \frac{d\delta}{dx} \sim \mathcal{L}v_n. \quad (2.2)$$

Sreenivasan *et al.* (1989) introduced and demonstrated the idea that the TNT interface is fractal with a well-defined fractal dimension, which in the case of our 2D planes would be the fractal dimension D of the TNT interfacial line in the plane, D being such that $1 \leq D < 2$. The length \mathcal{L} of the interfacial line in the 2D plane at x can therefore be estimated in terms of D , $\delta(x)$ and a characteristic thickness $\eta_I(x)$ of the interface as follows:

$$\mathcal{L} \sim \delta(\eta_I/\delta)^{1-D}. \quad (2.3)$$

To close equations (2.2) and (2.3) so that $v_n(x)$ can be obtained from $\delta(x)$ we follow Corrsin & Kistler (1955) and adopt $\eta_I \sim \nu/v_n$. This yields

$$v_n/U_\infty \sim \left(\frac{\delta U_\infty}{\nu}\right)^{\frac{1-D}{D}} \left(\frac{d\delta}{dx}\right)^{1/D}. \quad (2.4)$$

The dependence of the wake width δ on streamwise distance x is critically dependent on the scalings of the centreline turbulence dissipation rate $\epsilon_0(x)$ (see Vassilicos (2015); Dairay *et al.* (2015) and references therein). Dairay *et al.* (2015) showed, for the axisymmetric self-similar turbulent wake, that

$$\delta(x)/\theta \sim \left(\frac{x-x_0}{\theta}\right)^\beta \quad (2.5)$$

and

$$u_0(x)/U_\infty \sim \left(\frac{x-x_0}{\theta}\right)^\alpha \quad (2.6)$$

where θ is the momentum thickness, x_0 is a virtual origin, u_0 is the centreline velocity

[†] The word ‘‘suggest’’ can be replaced by the word ‘‘imply’’ if the interface has only one intersection with nearly every single radial line at nearly every single time in the 2D plane normal to the x -axis. In such a case, $A(x)$ is the time average of $\frac{1}{2} \int_0^{2\pi} R_I^2(\phi, x, t) d\phi$ where $R_I(\phi, x, t)$ describes the TNT interfacial curve in that 2D plane at x at time t . Given axisymmetry and ergodicity, it is then possible to write $A(x) = \pi \int_0^\infty R_I^2 P(R_I, x) dR_I$ which directly implies $A(x) \sim \delta^2(x)$ if $P(R_I; x) = \delta^{-1}p(R_I/\delta)$.

deficit; the exponents $\beta = -\alpha/2 = \frac{1+m}{3+m}$ are determined by the scalings of ϵ_0 , i.e.

$$\epsilon_0(x) \sim \left(\frac{U_\infty L_b}{\sqrt{K_0 \delta}}\right)^m K_0^{3/2} / \delta \quad (2.7)$$

where L_b is the size of the wake generator and K_0 is the centreline turbulent kinetic energy. The exponent $m = 0$ corresponds to the well-known classical scaling of the turbulence dissipation which is consistent with the Kolmogorov equilibrium theory (see Dairay *et al.* (2015) and Vassilicos (2015)). The exponent $m = 1$ corresponds to the non-equilibrium dissipation scalings found in various high Reynolds number turbulent flows (Vassilicos (2015), Goto & Vassilicos (2015)). And $m = 1/2$ is the exponent reported by Dairay *et al.* (2015); Dairay & Vassilicos (2016)) for the kind of moderate Reynolds number axisymmetric self-similar turbulent wakes which we study in the following section.

The scalings of v_n , obtained from (2.4) and (2.5), are given by

$$v_n/U_\infty \sim \left(\frac{U_\infty L_b}{\nu}\right)^{\frac{1-D}{D}} \left(\frac{x-x_0}{\theta}\right)^{-\gamma_e} \quad (2.8)$$

where $\gamma_e = \frac{\beta(D-1)}{D} + \frac{1-\beta}{D}$.

We need to compare these scalings with those of the Kolmogorov velocity $u_\eta \sim \nu/\eta_K \sim (\nu\epsilon_0)^{1/4}$ and to do this we need (2.7), (2.5) and the scalings of K_0 which can be obtained from (2.5), (2.6) and the Townsend-George relation[†] $K_0 \sim U_\infty u_0 d\delta/dx$ (see Dairay *et al.* (2015)). We obtain

$$u_\eta/U_\infty \sim \left(\frac{U_\infty L_b}{\nu}\right)^{-1/4} \left(\frac{x-x_0}{\theta}\right)^{-\gamma_\eta} \quad (2.9)$$

where $\gamma_\eta = \frac{\beta(1+m)}{4} + \left(\frac{3-m}{8}\right)(\beta+1)$.

The dissipation scaling (2.7) implied by the Kolmogorov equilibrium cascade phenomenology (see Vassilicos (2015), Dairay *et al.* (2015) and Obligado *et al.* (2016)) corresponds to $m = 0$ which implies $\beta = 1/3$ and therefore $\gamma_\eta = 7/12$ and $\gamma_e = (1+D)/3D$. There is one and only one value of D for which $\gamma_\eta = \gamma_e$ and therefore v_n/u_η is independent of x and this is $D = 4/3$. This value of D is also the one for which v_n and u_η have the same dependence on global Reynolds number $U_\infty L_b/\nu$. Interestingly, this value of D corresponds to the fractal dimension observed experimentally by Sreenivasan *et al.* (1989) and most recently by Mistry *et al.* (2016) in the far axisymmetric jet (see also references in Mistry *et al.* (2016) to other papers where such fractal dimension values are found). This value $4/3$ of D is a direct consequence of the Kolmogorov length-scale's $\nu^{3/4}$ dependence on ν as it also is in the arguments given for it by Sreenivasan *et al.* (1989).

In conclusion, if $m = 0$ and $D = 4/3$, then $v_n \sim u_\eta$ and $\eta_I = \nu/u_e \sim \eta_K$ in the sense that v_n and u_η on the one hand and η_I and η_K on the other have the same dependencies on $U_\infty L_b/\nu$ and x and therefore scale together. This is the case classically envisaged.

However, there are flow regions in various flows where the turbulence dissipation scaling is not the one implied by the Kolmogorov equilibrium cascade but has a new non-equilibrium form (see Vassilicos (2015), Goto & Vassilicos (2015), Dairay *et al.* (2015) and Obligado *et al.* (2016)). Such a flow region exists for example in high enough global Reynolds number self-similar axisymmetric turbulent wakes in the range of streamwise distances between about $10L_b$ and $O(100L_b)$ where the turbulence dissipation scales as

[†] This relation can actually not be found in Townsend (1976) and George (1989) but Townsend (1976) correctly predicted that K_0 is proportional to the Reynolds shear stress (the Townsend relation) and George (1989) was the first to predict that the Reynolds shear stress scales as $U_\infty u_0 d\delta/dx$ (the George relation). These two relations together give $K_0 \sim U_\infty u_0 d\delta/dx$ which was ironically predicted by neither Townsend (1976) nor George (1989) who had $K_0 \sim u_0^2$.

(2.7) with $m = 1$ (Dairay *et al.* (2015); Obligado *et al.* (2016); Dairay & Vassilicos (2016)). (The $m = 0$ scaling appears further downstream (Redford *et al.* (2012)) and for reasons different from the Kolmogorov equilibrium cascade, see Goto & Vassilicos (2016b).) The value $m = 1$ implies $\beta = 1/2$ and therefore $\gamma_\eta = 5/8$ and $\gamma_e = 1/2$ for any value of D . In this case

$$v_n/u_\eta \sim \left(\frac{U_\infty L_b}{\nu}\right)^{\frac{1-D}{D}+1/4} \left(\frac{x-x_0}{\theta}\right)^{1/8} \quad (2.10)$$

demonstrating clearly that the local entrainment velocity is fundamentally different from u_η . As in the previous case, though, v_n and u_η have the same Reynolds number dependence if $D = 4/3$ but not otherwise.

Interestingly, if one defines a Taylor length-scale velocity $u_\lambda = \nu/\lambda$ instead of $u_\eta = \nu/\eta_K$, and if one takes λ to scale according to $\epsilon_0 \sim \nu K_0/\lambda^2$ then (2.7), (2.5) and $m = 1$ yield $u_\lambda \sim \left(\frac{U_\infty L_b}{\nu}\right)^{-1/2} (L_b/\theta) \left(\frac{x-x_0}{\theta}\right)^{-1/2}$ which has the exact same dependence on x as v_n . The ratio v_n/u_λ is independent of x and depends on Reynolds number according to

$$v_n/u_\lambda \sim \left(\frac{U_\infty L_b}{\nu}\right)^{\frac{1-D}{D}+1/2}. \quad (2.11)$$

The implication for the characteristic thickness is $\eta_I = \nu/v_n \sim \lambda \left(\frac{U_\infty L_b}{\nu}\right)^{-(\frac{1-D}{D}+1/2)}$ where $\lambda \sim \left(\frac{U_\infty L_b}{\nu}\right)^{-1/2} \delta$. The thickness η_I is therefore effectively λ in the high Reynolds number non-equilibrium case $m = 1$ only if $D = 2$. Otherwise, η_I and λ have the same dependence on x but different dependencies on Reynolds number $\frac{U_\infty L_b}{\nu}$, in fact η_I/λ is an increasing function of $\frac{U_\infty L_b}{\nu}$ but $\eta_I/\delta \sim \left(\frac{U_\infty L_b}{\nu}\right)^{\frac{1-D}{D}}$ is a decreasing function of $\frac{U_\infty L_b}{\nu}$.

The conclusion is that, when $m = 1$, the characteristic thickness η_I sits between λ and δ and grows with x in the same way as λ .

3. DNS of an axisymmetric turbulent wake

In this section we test the assumptions made and results obtained in the previous section with a DNS of a spatially developing axisymmetric turbulent wake generated by a bluff plate placed normal to the incoming laminar free stream. The length L_b is the square root of the area of the plate. In such wakes, the turbulence is clearly axisymmetric for $x/L_b \geq 5$ and the profiles of the mean flow, turbulent kinetic energy, turbulence dissipation and Reynolds shear stress are self-similar for x/L_b larger than 10 or 20 (see Dairay *et al.* (2015); Dairay & Vassilicos (2016)). The relations (2.5), (2.6) and (2.7) are therefore valid for $x/L_b \geq 10$ and, more specifically, the turbulence dissipation scaling is given by (2.7) with $m = 1$ in the range $x/L_b = 10$ to $x/L_b = O(100)$ provided that the Reynolds number $\frac{U_\infty L_b}{\nu}$ is large enough, for example 40000 as in the laboratory experiments of Nedić *et al.* (2013), Dairay *et al.* (2015) and Obligado *et al.* (2016). At normalised distances x/L_b beyond $O(100)$ one expects to find (2.7) with $m = 0$ as suggested by the DNS of temporally evolving wakes of Redford *et al.* (2012).

Unfortunately, current state-of-the-art DNS of spatially developing axisymmetric turbulent wakes cannot reach such high Reynolds numbers and such far downstream distances. The massively parallel such DNS of Dairay *et al.* (2015) reached $\frac{U_\infty L_b}{\nu} = 5000$ and $x/L_b = 100$ with about 10^9 grid points. The spatial resolution $\Delta x = \Delta y = \Delta z = L_b/32$ of the DNS's uniform Cartesian grid was always below $4\eta_K$ between $x/L_b = 10$ and $x/L_b = 100$. The results for $m = 0$ and $m = 1$ of the previous section are therefore beyond the reach of such DNS. However, in their moderate Reynolds number turbulent wake, Dairay *et al.* (2015) reported an intermediate dissipation scaling (2.7) with $m = 1/2$ between $x/L_b = 50$ and $x/L_b = 100$. In this work we use the exact same DNS code and

	β	α	γ_η	γ_e
$m = 0$	1/3	-2/3	7/12	$\frac{1+D}{3D}$
$m = 1/2$	3/7	-6/7	≈ 0.61	$\frac{3}{7} + \frac{1}{7D}$
$m = 1$	1/2	-1	5/8	1/2

TABLE 1. Values of the exponents β in equation (2.5), α in equation (2.6), γ_η in equation (2.9) and γ_e in equation (2.8) for different turbulence dissipation scalings (2.7): $m = 0$ in the classical scaling case, $m = 1/2$ in the moderate Reynolds number non-equilibrium case and $m = 1$ in the high Reynolds number non-equilibrium case. D is the fractal dimension of the TNT interfacial line in the $y - z$ plane; $1 \leq D < 2$.

same flow configuration and parameters as Dairay *et al.* (2015) to test the assumptions made and results obtained in the previous section in the range $50 \leq x/L_b \leq 100$ and for $m = 1/2$. Dairay *et al.* (2015) validated their simulations of spatially developing axisymmetric turbulent wakes against experimental data.

The previous section's relations (2.5) to (2.9) remain valid for $m = 1/2$ but with $\beta = 3/7$, $\gamma_e = 3/7 + 1/(7D)$ and $\gamma_\eta \approx 0.61$ (see table 1). In this section we use the DNS to verify our assumptions (i) $P(R_I; x) = \delta^{-1}p(R_I/\delta)$ and $A \sim \delta^2$ (subsection 3.1) and (ii) the fractal nature of the TNT interface with (2.3) and $\eta_I \sim \nu/v_n$ (subsection 3.2); and to test our results (2.8) with $\gamma_e = 3/7 + 1/(7D)$ and (2.9) with $\gamma_\eta \approx 0.61$ (subsection 3.3).

A detailed description of the DNS code and flow configuration is given in Dairay *et al.* (2015) and references therein and we do not repeat it here for economy of space. The incompressible Navier-Stokes equations are solved with the massively parallel version of the code **Incompact3d** which is based on sixth-order compact schemes for spatial discretisation on a Cartesian mesh and a third-order Adams-Bashforth scheme for time advancement. An immersed boundary method is used to model the wake-generating bluff plate following the procedure of Parnaudeau *et al.* (2008). The plate is the same as the one used in the DNS and experiments of Dairay *et al.* (2015) and Nedić *et al.* (2013): it has an irregular (fractal-like) periphery which results in higher local Reynolds numbers in the flow for the same global Reynolds number $\frac{U_\infty L_b}{\nu}$. In the present case, the local Taylor length-based Reynolds number Re_λ varies slowly and remains close to 55 throughout the range $50 \leq x/L_b \leq 100$. The DNS of Goto & Vassilicos (2015) suggest that the non-equilibrium dissipation exponent $m = 1$ appears most clearly at values of Re_λ larger than about 100 or so. The absence of $m = 1$ in the present DNS and those of Dairay *et al.* (2015); Dairay & Vassilicos (2016) is consistent with this observation.

We adopt inflow/outflow boundary conditions in the streamwise direction with uniform streamwise velocity U_∞ without turbulence at the inlet and a one-dimensional convection equation at the outlet. The streamwise and two lateral directions are all orthogonal to each other and the streamwise size of the computational domain is $L_x = 120L_b$ whereas the lateral sizes are $L_y = L_z = 15L_b$. The plate is located at a distance $10L_b$ from the inlet. We collect several variables, including the instantaneous fluid velocity components u in the x direction, v in the y direction and w in the z direction and the modulus ω of the instantaneous vorticity vector $\nabla \times (u, v, w)$ at every grid point of seventeen lateral planes separated by a streamwise distance $5L_b$ from $x/L_b = 20$ to $x/L_b = 100$. These planar data are collected every fifth time step in a simulation run of 200000 time steps

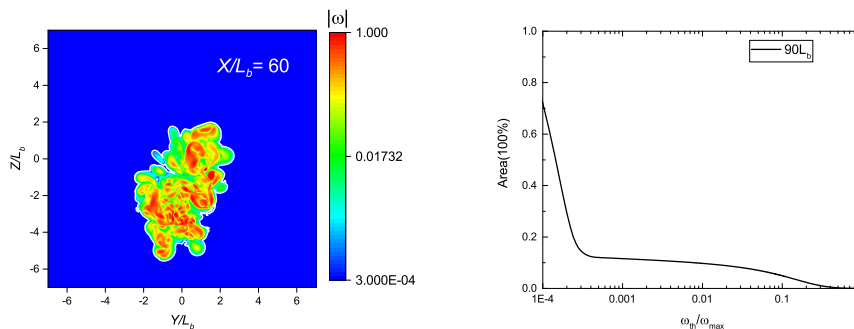


FIGURE 1. Definition of interface with examples of the ω field in a $y-z$ plane (left) and $A/(L_y L_z)$ versus ω_{th}/ω_{max} (right). The two plots are given at two different values of x/L_b ($x/L_b = 60$ on the left and $x/L_b = 90$ on the right) to give a feel of the fact that the interface is well-defined at all the values of x/L_b considered here. These plots are very similar at all streamwise positions where we saved planar data.

which corresponds to approximately 109 vortex shedding periods. The initial condition of our simulation is a fully developed instantaneous field obtained and stored by Dairay *et al.* (2015).

3.1. DNS results: radial position of interface and area of turbulent region

We define the intersection between the TNT interface and one of our 2D planar cuts in effectively the same way that various authors have defined the TNT interface in terms of a volume fraction in 3D space (see da Silva *et al.* (2014), Watanabe *et al.* (2015), Watanabe *et al.* (2016)). We define the area A_t containing all the points in the $y-z$ plane where ω is larger than a certain threshold ω_{th} at time t . Figure 1(left) shows an example of an instantaneous snapshot of the ω field in the $y-z$ plane at $x/L_b = 60$. Similar ω field snapshots can be obtained at other x/L_b locations. The area A_t takes different values for different choices of ω_{th} , but the presence of the TNT interface means that A_t will be approximately constant over a significant range of thresholds. Figure 1(right) is a plot of A (normalised by $L_y L_z$ so as to have an area fraction) defined as the time-average of A_t conditional on $\omega_{th}(t)/\omega_{max}(t)$ where $\omega_{max}(t)$ is the maximum value of ω at time t in the plane considered and where $\omega_{th}(t)/\omega_{max}(t)$ is kept constant even though $\omega_{max}(t)$ varies with t . Plots of instantaneous values of $A_t/(L_y L_z)$ versus $\omega_{th}/\omega_{max}(t)$ look very similar. A plateau is clearly visible in figure 1(right) between $\omega_{th}/\omega_{max} = 4 \cdot 10^{-4}$ and 10^{-2} . A similar plateau is also clearly present at all the other streamwise locations where we saved planar data, however over slightly different ranges of ω_{th}/ω_{max} for different locations (e.g. between $2 \cdot 10^{-4}$ and 10^{-2} at $x/L_b = 50$). (We have repeated the exact same procedure with $\omega_{th}(t)/\omega_{av}(t)$ where $\omega_{av}(t)$ is the instantaneous average of ω in the $y-z$ plane considered, and with $\omega_{th}/\bar{\omega}(x, 0, 0)$ where $\bar{\omega}(x, 0, 0)$ is the time-average of ω at the intersection of the centreline and the $y-z$ plane considered and all our results in this paper remain the same except that the actual values of $\omega_{th}(t)/\omega_{max}(t)$, $\omega_{th}(t)/\omega_{av}(t)$ and $\omega_{th}/\bar{\omega}(x, 0, 0)$ are of course different.)

Given the plateau in plots such as figure 1(right), it is possible to define the TNT interface location in a $y-z$ plane with any normalised threshold $\omega_{th}(t)/\omega_{max}(t)$ between $4 \cdot 10^{-4}$ and 10^{-2} . Once such a threshold has been chosen, it is then possible to obtain the radial positions $R_I(x, \phi, t)$ of the interface from its intersections with radial straight lines at various azimuthal angles ϕ in the $y-z$ plane at x . These radial straight lines start from the centreline's position $y = z = 0$ in this plane. Relatively rarely is there

more than one intersection between one of these straight lines and the TNT interface. In such cases the value of R_I that we take is the largest one.

Statistics of R_I at a given streamwise location x/L_b can be obtained by sampling over ϕ and time t . An example is the average interfacial radius $\overline{R_I}(x)$ which is a function only of x (averages over ϕ and t having been taken). An example of such average interfacial radii is give in figure 2(left). For this plot, the threshold defining the TNT interface is $\omega_{th}/\omega_{max} = 4 \cdot 10^{-4}$ but we have checked that $\overline{R_I}(x)$ does not vary significantly if larger values of this normalised threshold are chosen up to about $7 \cdot 10^{-3}$.

Figure 2(left) concentrates attention in the range $x/L_b = 50$ to 100 where Dairay *et al.* (2015) found the $m = 1/2$ dissipation scaling and shows that $\overline{R_I}(x) \sim \delta(x)$ in agreement with original claims by Corrsin & Kistler (1955). More specifically,

$$\overline{R_I}(x) \approx 1.6\delta(x) \quad (3.1)$$

in our case.

The definition of the wake width of an axisymmetric turbulent wake is

$$\delta^2(x) = \frac{1}{u_0} \int_0^\infty (U_\infty - U)rdr \quad (3.2)$$

where $U = \bar{u}$ is the mean streamwise velocity averaged over ϕ and t and therefore function of x and radius r , and $u_0(x)$ equals $U_\infty - U(x, r = 0)$ where $r = 0$ marks the intersection of the plane with the centreline. Following the practical procedure taken in Dairay *et al.* (2015) the integral in (3.2) is carried out up to $r = 7L_b$, and U_∞ in $u_0(x)$ and in (3.2) is replaced by $\bar{u}(x, r = 7L_b)$. This takes care of the finite size of the computational domain and avoids negative values of $U_\infty - U$. The plots in figure 2, where both $\overline{R_I}(x)$ and A are normalised by $\delta(x)$, are obtained with this procedure for $\delta(x)$ as are all other plots in this paper where $\delta(x)$ is required.

Figure 2 supports both scalings, $\overline{R_I}(x) \approx 1.6\delta(x)$ and $A(x) \sim \delta^2(x)$, the latter scaling being an important assumption in the theoretical arguments of section 2. The quality of these scalings does not change significantly with normalised threshold ω_{th}/ω_{max} . More generally, we find that the PDF $P(R_I; x)$ takes a self-similar form normalised by $\delta(x)$ in the investigated range $50 \leq x/L_b \leq 100$ (see figure 3), namely

$$\delta(x)P(R_I; x) = p(R_I/\delta(x)) \quad (3.3)$$

where the function $p(R_I/\delta(x))$ is well approximated by a Gaussian of $\frac{R_I}{\delta(x)} - 1.6$ with a variance of 1.1 in the range $-3/2 < \frac{R_I}{\delta(x)} - 1.6 < 3/2$. Corrsin & Kistler (1955) were the first to suggest that this PDF may have an approximate Gaussian form.

Figure 3 includes two plots, one of $P(R_I; x)$ versus R_I at different values of x/L_b and one of $\delta(x)P(R_I; x)$ versus $R_I/\delta(x)$ which demonstrates the collapse according to (3.3). These particular plots have been obtained with normalised thresholds ω_{th}/ω_{max} which vary between $6 \cdot 10^{-4}$ and 10^{-3} at different streamwise positions x/L_b for reasons which are explained in subsection 3.2. However there is no appreciable difference if these plots are obtained with the same threshold for all streamwise locations as long as ω_{th}/ω_{max} is chosen between $4 \cdot 10^{-4}$ and $7 \cdot 10^{-3}$.

3.2. DNS results: fractal nature of the TNT interface and $\eta_I \sim \nu/v_n$

We now test the assumption that the intersection of the TNT interface with a $y - z$ plane is a fractal line over some range of length-scales. To test this assumption we use the well-known box-counting algorithm (Mandelbrot (1982), Sreenivasan *et al.* (1989), Mistry *et al.* (2016)) and count the number of squares of side-size η_B required to cover the TNT interfacial line in the 2D plane. We repeat this counting for about a fifth of all

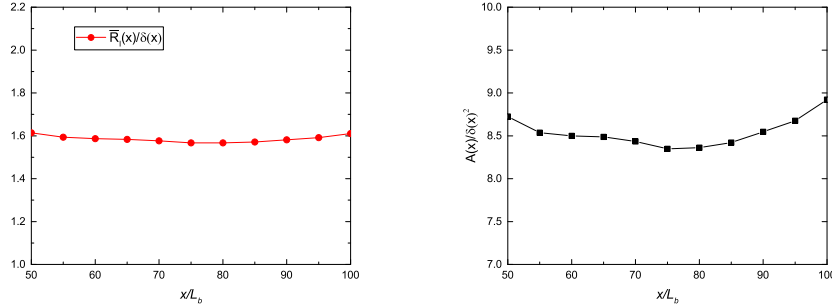


FIGURE 2. $\overline{R_I(x)}/\delta(x)$ (left) and $A(x)/\delta^2(x)$ (right) versus x/L_b . These plots were obtained with $\omega_{th}/\omega_{max} = 4 \cdot 10^{-4}$ at all x .

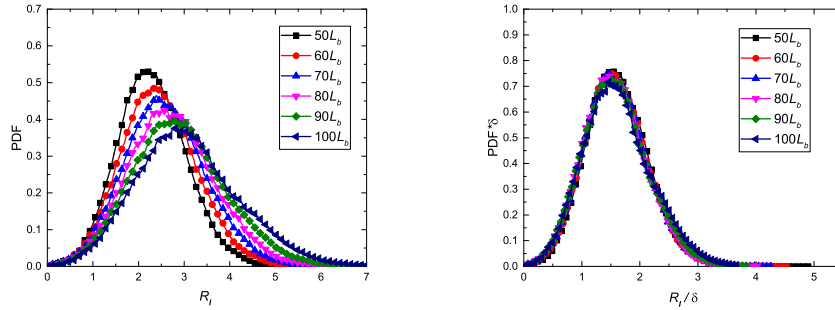


FIGURE 3. Interfacial radial location PDF: $P(R_I; x)$ versus R_I at different values of x/L_b (left) $\delta(x)P(R_I; x)$ versus $R_I/\delta(x)$ (right) for different values of x/L_b . The normalised threshold ω_{th}/ω_{max} used to define the TNT interface at each x/L_b varies between $6 \cdot 10^{-4}$ and 10^{-3} according to figure 5(left). There is no appreciable difference if these plots are obtained with the same ω_{th}/ω_{max} at all x/L_b as long as ω_{th}/ω_{max} is chosen between $4 \cdot 10^{-4}$ and $7 \cdot 10^{-3}$ (see figure 1).

our time-samples and then calculate the average number of such squares of size η_B . This average number is $N(\eta_B)$ and it is obtained for a range of η_B values from η_K to a few times δ . An example of the outcome of this procedure is given in figure 4(left).

For all the 2D planes between $x/L_b = 50$ and 100 tried here, there is a well-defined range of sizes η_B where $N(\eta_B)$ can be fitted as $N(\eta_B) = N_\delta(\eta_B/\delta)^{-D}$ with $D > 1$. The exponent D is the fractal dimension of the TNT interfacial line in the 2D $y - z$ plane and we find it to be equal to $6/5 \pm 0.02$ at all the streamwise locations that we have interrogated (see figure 4). At smaller length-scales η_B , the dimension D is close to 1 as it should be. This finding supports the assumption that the TNT interfacial line is fractal in every 2D lateral plane between $x/L_b = 50$ and 100. Its non-integer fractal dimension is defined over a range of scales which spans one decade. †

Even though $D = 6/5 \pm 0.02$ irrespective of streamwise position in the streamwise range tested, N_δ varies significantly with x if we keep the value of ω_{th}/ω_{max} the same for all our

† We checked that the TNT interface is equally wrinkled in parts of $x - y$ and $x - z$ planes extending from $x/L_b = 50$ to $x/L_b = 100$ by confirming that the fractal dimension of the TNT interfacial line in such planes is also well defined over an equally broad range of scales and also equal to $6/5 \pm 0.02$.

2D planes (the same happens when we use ω_{th}/ω_{av} or $\omega_{th}/\bar{\omega}(x, 0, 0)$ instead of ω_{th}/ω_{max}). There is no irrefutable reason why the downstream evolution of the interface should be traced with the same threshold ω_{th}/ω_{max} (or ω_{th}/ω_{av} or $\omega_{th}/\bar{\omega}(x, 0, 0)$) at all streamwise positions x . The dynamics of the interfacial region are actually such that the normalised threshold range over which the time-average area A has a plateau in figure 1(right) varies a little with x and ω_{max} varies with both time and x too. However, N_δ should remain constant with x for a self-similar turbulent wake. We therefore identify a set of different normalised thresholds ω_{th}/ω_{max} for different streamwise positions, see figure 5(left), for which N_δ is approximately constant, see figure 5(right). These normalised thresholds are all within the minimal range $4 \cdot 10^{-4}$ and $7 \cdot 10^{-3}$ which is part of the range where A has a plateau for any x/L_b between 50 and 100. We have checked that the value of D remains within $6/5 \pm 0.02$ with these thresholds. (The results are effectively the same if ω_{th}/ω_{av} or $\omega_{th}/\bar{\omega}(x, 0, 0)$ is used instead of ω_{th}/ω_{max} with a similar variation in ω_{th}/ω_{av} and $\omega_{th}/\bar{\omega}(x, 0, 0)$ by a factor of about less than 2 but different actual values for ω_{th}/ω_{av} or $\omega_{th}/\bar{\omega}(x, 0, 0)$.)

The fractal nature of the TNT interfacial line enters the theoretical considerations of section 2 via the length \mathcal{L} in equations (2.3) and (2.2). We therefore calculate an estimate of the time-averaged interfacial length at resolution η_B . This is $L(\eta_B) = \eta_B N(\eta_B)$ and an example is given in figure 4(right). A maximum value of $\ln L(\eta_B)$ is clearly visible in figure 4(right) and it is present at all streamwise positions. This maximum demarcates the scales η_B which are small enough to resolve the line as a set of points from the scales η_B which are large enough for the line to be perceived as continuous. We take this maximum value of $L(\eta_B)$ to be the actual time-average length of the interface \mathcal{L} . (We verified this way of estimating \mathcal{L} against a way based on the marching squares algorithm, fully independently of the box-counting algorithm, and found good agreement.) In figure 6(left) we plot $\mathcal{L}(x)/L_b$ as a function of x/L_b . We find, as expected, that \mathcal{L} is an increasing function of x .

Equation (2.3) in section 2 follows from $\mathcal{L} \sim L(\eta_B)$ for $\eta_B = \eta_I$. Indeed, $\mathcal{L} \sim L(\eta_I) = \eta_I N(\eta_I)$, $N(\eta_I) = N_\delta (\eta_I/\delta)^{-D}$ and $N_\delta = Const$ yield (2.3). But the other important assumption in section 2 is that $\mathcal{L} \sim L(\eta_I)$ with $\eta_I \sim \nu/v_n$. To verify this assumption, we calculate v_n from equation (2.2) with \mathcal{L} estimated as described in the previous paragraph. We then calculate $L(\eta_I) = \eta_I N(\eta_I) = N_\delta \delta (\eta_I/\delta)^{1-D}$ with $\eta_I = \nu/v_n$ and compare it to \mathcal{L} . The results of this comparison are given in figure 6. We find that $\mathcal{L}/L(\eta_I)$ is approximately constant with x , in support of the way we use $\eta_I \sim \nu/v_n$.

In conclusion, our DNS supports all the assumptions made in section 2, in particular $A \sim \delta^2$ (as shown in subsection 3.1) and $\mathcal{L} \sim \delta (\eta_I/\delta)^{1-D}$ with $\eta_I \sim \nu/v_n$. The actual value of η_I for which \mathcal{L} is equal (rather than just proportional) to $L(\eta_I)$ is a value close to λ as can be inferred from figure 4. However, η_I does not scale with λ (nor does it scale with η_K) but with ν/v_n . We checked that $(\nu/v_n)/\lambda$ and $(\nu/v_n)/\eta_K$ are not constant and in fact vary significantly with x . The range of length-scales where the TNT interfacial line in the 2D planes $x/L_b = 50$ to 100 is fractal is bound from below by an inner length-scale proportional to ν/v_n and from above by a multiple of δ .

3.3. DNS results: Kolmogorov and local entrainment velocities

Having found DNS support for the assumptions made in section 2 we now use our DNS to assess the main results of the theoretical arguments in that section, namely equations (2.8) and (2.9). As shown by Dairay *et al.* (2015), the dissipation scaling in the range $x/L_b = 50$ to 100 of the axisymmetric turbulent wake of our DNS is such that $m = 1/2$ which mean that we need to assess equations (2.8) and (2.9) against our DNS results with $\gamma_e = 3/7 + 1/(7D)$ for (2.8) and $\gamma_\eta \approx 0.607$ for (2.9) (see table 1). Indeed, $m = 1/2$ implies

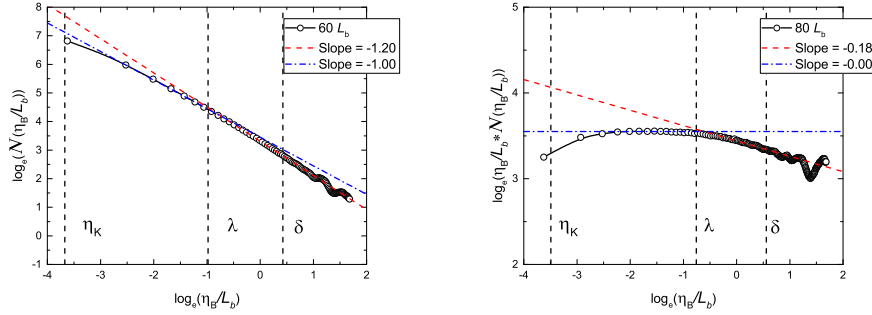


FIGURE 4. Time-average number $N(\eta_B)$ of squares of side-size η_B needed to cover the TNT interfacial line in the 2D plane $x/L_b = 60$ versus η_B/L_b (left) and $\eta_B N(\eta_B)$ versus η_B/L_b for the 2D plane $x/L_b = 80$ (right). The left and right $\ln - \ln$ plots are given for different streamwise positions to give an impression of variability. The fractal dimension is well-defined over one decade and found to equal $6/5 \pm 0.02$ in the range $x/L_b = 50$ to $x/L_b = 100$. The values $\eta_B = \eta_K$, λ and δ are indicated in the plots for reference.

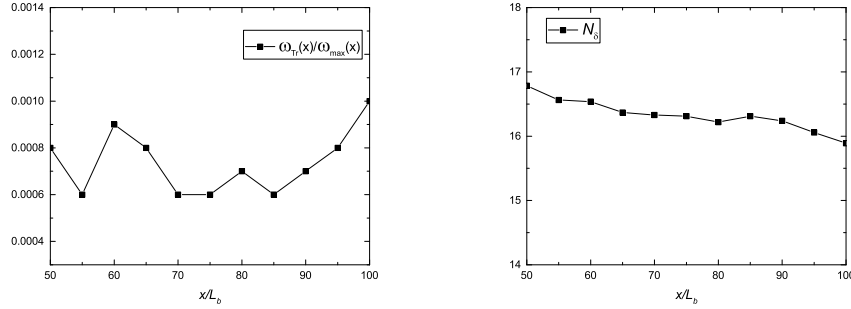


FIGURE 5. Choice of thresholds ω_{th}/ω_{max} (left plot as a function of x/L_b) so that N_δ (right plots as a function of x/L_b) remains approximately constant with x .

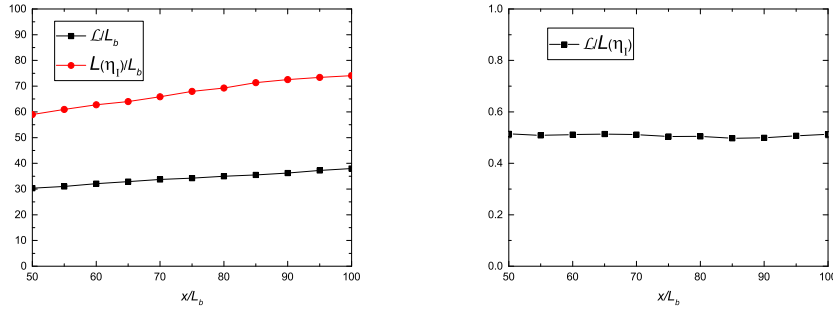


FIGURE 6. \mathcal{L}/L_b and $L(\eta_I)/L_b$ (left) and $\mathcal{L}/L(\eta_I)$ (right) versus x/L_b . The TNT interfacial line is defined with the thresholds given in figure 5(left) and $\eta_I = \nu/v_n$ where v_n is calculated from (2.2).

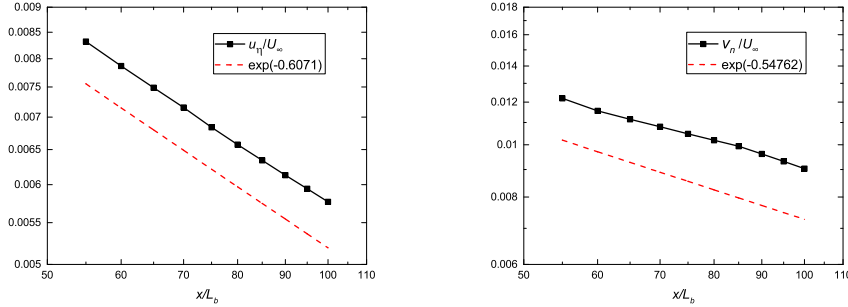


FIGURE 7. u_n/U_∞ (left) and v_n/U_∞ (right) versus x/L_b . For comparison the dotted line in the left plot represents the power law dependence on x given by (2.9) with $\gamma_\eta \approx 0.607$ and the dotted line in the right plot represents the power law dependence on x given by (2.8) with $\gamma_e = 3/7 + 1/(7D)$ and $D = 6/5$.

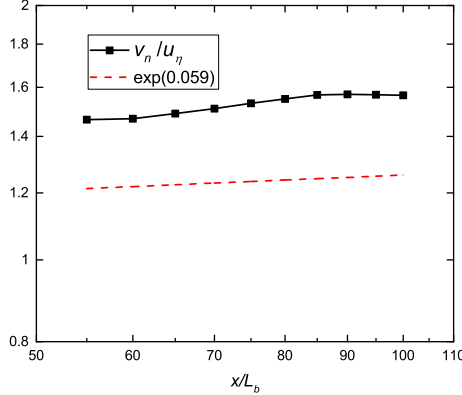


FIGURE 8. v_n/u_η versus x/L_b . For comparison the dotted line represents $(x - x_0)^{\gamma_\eta - \gamma_e} = (x - x_0)^{0.059}$ which is the x -dependence predicted for v_n/u_η from (2.8) and (2.9) if $m = 1/2$, $D = 6/5$ and x_0 is the same virtual origin as the one in (2.5) and (2.6).

$\beta = 3/7$ which implies $\gamma_e = \frac{\beta(D-1)}{D} + \frac{1-\beta}{D} = 3/7 + 1/(7D)$ and $\gamma_\eta = \frac{\beta(1+m)}{4} + \frac{3-m}{8}(\beta+1) \approx 0.607$.

Figure 7(left) shows that the DNS returns an x -dependence of u_n/U_∞ which is in good agreement with (2.9) and $\gamma_\eta = 0.607$ in the range $x/L_b = 50$ to 100 . However, as can be seen in figure 7(right), the agreement between (2.8) with $\gamma_e = \frac{\beta(D-1)}{D} + \frac{1-\beta}{D} = 3/7 + 1/(7D) = 0.5476$ (for $D = 6/5$) and the DNS is less good even though the decreasing downstream nature of v_n/U_∞ is well captured and is not too far from the data. These data have been produced by calculating the local entrainment velocity v_n from (2.2), (2.5) and the previous subsection's DNS estimate of \mathcal{L} . The agreement with (2.8) where $\gamma_e = 0.5476$ cannot be expected to be too good given that D varies around $6/5$ from one streamwise position to the other and given the uncertainty on how to exactly follow the TNT interfacial line in terms of vorticity thresholds from one streamwise position to the other. Even so, the prediction that v_n/u_η is not constant but a very slowly increasing function of x is supported by our DNS (see figure 8).

4. Conclusion and discussion

It is not always true that the local entrainment velocity v_n scales with the Kolmogorov velocity u_η . As we have argued in this paper, this depends on the turbulence dissipation scalings, at least in the case of self-similar axisymmetric turbulent wakes.

Recent studies have shown that the local entrainment velocity scales with the Kolmogorov velocity and that the thickness of the TNT interface scales with the Kolmogorov length-scale in some turbulent flows (Holzner & Lüthi (2011), Watanabe *et al.* (2015), Watanabe *et al.* (2016)). This conclusion may have been reached because the regions of the flows studied are such that the turbulence dissipation scalings are classical, as one may for example expect extremely far downstream in a turbulent wake (Redford *et al.* (2012)), or because the effect can be imperceptible (see figure 8), as in nearer field axisymmetric self-similar turbulent wakes when the Reynolds number is not high enough.

Our DNS study has concentrated in a region of a turbulent wake where the turbulent flow is statistically axisymmetric and self-similar and where the dissipation scalings are given by (2.7) with $m = 1/2$. We have presented theoretical arguments which demonstrate that the local entrainment velocity and the thickness of the TNT interface do indeed scale with the Kolmogorov velocity and length-scale respectively when $m = 0$. This is the dissipation scaling usually considered, for example in textbooks (e.g. Tennekes & Lumley (1972), Townsend (1976), Pope (2000)). However, the same theoretical arguments lead to the conclusion that v_n does not scale with u_η when $m \neq 0$ and that v_n has the same dependence on downstream streamwise distance as ν/λ when $m = 1$ even though it has a different dependence on global Reynolds number. The case $m = 1$ corresponds to the non-equilibrium dissipation scaling found in various turbulent flows at high enough Reynolds numbers (Vassilicos (2015); Goto & Vassilicos (2015); Obligado *et al.* (2016)).

Our theoretical arguments have been based on the idea, already present in Corrsin & Kistler (1955), that interfacial statistics scale with the wake width $\delta(x)$ and in particular that the time-averaged area A of the fully turbulent region in a plane normal to the mean direction of the flow scales with δ^2 . Our DNS data have provided good support for $A \sim \delta^2$ in the range $50 \leq x/L_b \leq 100$. This is the first time that such a result has been obtained by any means, whether experimental or numerical. We have also shown that the PDF of the radial interface location is self-similar and scales with δ , at least in that range. This kind of result finds its roots in Corrsin & Kistler (1955) and has been verified in various flows since then, such as turbulent jets (Watanabe *et al.* (2014), Mistry *et al.* (2016)) and turbulent mixing layers (Attili *et al.* (2014)) but this is the first time that it has been obtained in a DNS of a spatially evolving turbulent wake. Furthermore, we find that the PDF of the radial interface location is approximately Gaussian in our flow, in agreement with the original suggestion by Corrsin & Kistler (1955) and with similar findings in various other turbulent flows including time-evolving wakes (Bisset *et al.* (2002)), turbulent boundary layers (Chauhan *et al.* (2014), Borrell & Jiménez (2016)), turbulent jets (Westerweel *et al.* (2009), Watanabe *et al.* (2014), Gampert *et al.* (2014), Mistry *et al.* (2016)) and turbulent mixing layers (Attili *et al.* (2014)).

The other important assumption of our theoretical arguments is that the TNT interfacial line in 2D planes normal to the mean direction of the flow has fractal properties. Our DNS has provided support for this assumption and has returned a fractal dimension $D = 6/5 \pm 0.02$ at the streamwise locations $x/L_b = 50$ to 100 where our DNS study has concentrated attention. The DNS results also support the scaling of the relevant inner length-scale η_I with ν/v_n , somehow echoing the arguments of Corrsin & Kistler (1955).

It is interesting that D is appreciably different from the more usual value $4/3$ which follows from a Kolmogorov scaling of the TNT interface (see paragraph under equation

(2.9) in section 2). This finding is consistent with the non-Kolmogorov scalings of the TNT interface when $m \neq 0$. In the flow region studied by our DNS, $m = 1/2$. In the same flow region, $m = 1$ when the Reynolds number is sufficiently higher (see Vassilicos (2015), Dairay *et al.* (2015), Oblgado *et al.* (2016)).

In the DNS of Redford *et al.* (2012) and Goto & Vassilicos (2016b) and the wind tunnel experiments of Valente & Vassilicos (2012, 2014) the dissipation scaling morphs quite suddenly from $m = 1$ to $m = 0$ far enough downstream. The DNS of decaying periodic turbulence of Goto & Vassilicos (2016b) suggest that this happens when the large-scale coherent structures weaken enough for their presence to stop affecting turbulence statistics significantly. This suggests that different local TNT interface scalings for v_n and η_I may exist in the presence or absence of engulfment (see Corrsin & Kistler (1955), da Silva *et al.* (2014)), and that engulfment may be closely related to non-equilibrium turbulence cascade and associated dissipation scaling exponents $m \neq 0$, in particular $m = 1$, whereas the prevalence of nibbling (see Corrsin & Kistler (1955), da Silva *et al.* (2014)) may be associated with the usual dissipation scaling exponent $m = 0$. We are currently pursuing this new research direction and hope to report on it soon.

Acknowledgements

We thank Dr Maarten van Reeuwijk and Professor Yasuhiko Sakai for their helpful comments on the manuscript. We acknowledge the UK Turbulence Consortium for HPC resources on ARCHER (UK) and ERC Advanced grant 320560 awarded to J.C. Vassilicos.

Appendix A

In this appendix we present the proof of equation (2.1) and the related exact meaning in which v_n is an average local propagation velocity.

Integrating the incompressibility condition over the 2D region inside an iso-entrophy line in the $y - z$ plane at a given streamwise coordinate x we have

$$\int_{\mathcal{A}_t(x)} \left(\frac{\partial u}{\partial x} + \frac{\partial v}{\partial y} + \frac{\partial w}{\partial z} \right) dydz = 0 \quad (\text{A } 1)$$

where $\mathcal{A}_t(x)$ is the region of the 2D plane covering the higher entrophy side of the iso-entrophy line considered. The surface area of this region is $A_t(x) = \int_{\mathcal{A}_t(x)} dydz$. Using

Gauss's divergence theorem in the $y - z$ plane we get

$$\int_{\mathcal{A}_t(x)} \frac{\partial u}{\partial x} dydz = - \int_{\mathcal{A}_t(x)} \left(\frac{\partial v}{\partial y} + \frac{\partial w}{\partial z} \right) dydz = - \int_{\partial \mathcal{A}_t(x)} (v, w) \cdot \mathbf{n} dl \quad (\text{A } 2)$$

where \mathbf{n} is the 2D unit vector in the $y - z$ plane that is normal to the iso-line defining the border $\partial \mathcal{A}_t(x)$ of the 2D region $\mathcal{A}_t(x)$ and pointing outwards.

Defining the normal fluid velocity $V_f \equiv (v, w) \cdot \mathbf{n}$ and the average normal fluid velocity $\tilde{V}_f \equiv \mathcal{L}_t^{-1} \int_{\partial \mathcal{A}_t(x)} V_f dl$ where \mathcal{L}_t is the instantaneous length of the iso-entrophy line $\partial \mathcal{A}_t(x)$, (A2) becomes

$$\int_{\mathcal{A}_t(x)} \frac{\partial u}{\partial x} dydz = -\mathcal{L}_t \tilde{V}_f. \quad (\text{A } 3)$$

Clearly, \tilde{V}_f is the average of V_f over the instantaneous iso-entrophy line $\partial \mathcal{A}_t(x)$ and is, as such, a function of time t and streamwise position x .

We now seek a formula for $\frac{d}{dx} \int_{\mathcal{A}_t(x)} u dydz$:

$$\begin{aligned} \frac{d}{dx} \int_{\mathcal{A}_t(x)} u dydz &= \lim_{\delta x \rightarrow 0} \frac{1}{\delta x} \left(\int_{\mathcal{A}_t(x+\delta x)} u(x+\delta x) dydz - \int_{\mathcal{A}_t(x)} u(x) dydz \right) \\ &= \int_{\mathcal{A}_t(x)} \frac{\partial u}{\partial x} dydz + \lim_{\delta x \rightarrow 0} \frac{1}{\delta x} \left(\int_{\mathcal{A}_t(x+\delta x)} u(x+\delta x) dydz - \int_{\mathcal{A}_t(x)} u(x+\delta x) dydz \right). \end{aligned} \quad (\text{A } 4)$$

The bracketed term in the second line of (A4) is the difference between the surface integrals of $u(x+\delta x)$ over $\mathcal{A}_t(x+\delta x)$ and $\mathcal{A}_t(x)$ respectively. The difference between these two surface integrals is, to leading order, equal to the curvilinear integral $\int_{\partial \mathcal{A}_t(x)} u V_n \delta t dl$ where $\delta t \equiv \delta x/u$ and V_n is the instantaneous local velocity of the iso-line $\partial \mathcal{A}_t(x)$ normal to itself in the $y-z$ plane at x . Hence, (A4) becomes

$$\frac{d}{dx} \int_{\mathcal{A}_t(x)} u dydz = \int_{\mathcal{A}_t(x)} \frac{\partial u}{\partial x} dydz + \int_{\partial \mathcal{A}_t(x)} V_n dl. \quad (\text{A } 5)$$

Making use of (A3) and defining the average normal propagation velocity $\tilde{V}_n \equiv \mathcal{L}_t^{-1} \int_{\partial \mathcal{A}_t(x)} V_n dl$ leaves us with

$$\frac{d}{dx} \int_{\mathcal{A}_t(x)} u dydz = \mathcal{L}(t)(\tilde{V}_n - \tilde{V}_f). \quad (\text{A } 6)$$

Both \tilde{V}_n and \tilde{V}_f are functions of x and t and $\tilde{V}_n - \tilde{V}_f$ is the line-averaged propagation velocity of the iso-line $\partial \mathcal{A}_t(x)$ relative to the fluid. Averaging over time both sides of (A6) and using the Reynolds decomposition $u = \langle u \rangle + u'$ yields

$$\frac{d}{dx} \langle \int_{\mathcal{A}_t(x)} u dydz \rangle = \langle \mathcal{L}(t)(\tilde{V}_n - \tilde{V}_f) \rangle \quad (\text{A } 7)$$

where $\langle \rangle$ denotes time average. (We set $\langle \int_{\mathcal{A}_t(x)} u' dydz \rangle = 0$ and confirmed that this is indeed a very good approximation in our DNS, in fact increasingly so with increasing x/L_b as the ratio of $\langle \int_{\mathcal{A}_t(x)} u' dydz \rangle$ to $\langle \int_{\mathcal{A}_t(x)} \langle u \rangle dydz \rangle$ is less than $7 \cdot 10^{-3}$ at $x/L_b = 50$ and about $4 \cdot 10^{-3}$ at $x/L_b = 100$.) At $x/L_b \gg 1$, $\langle u \rangle - U_\infty \ll U_\infty$, as for example confirmed by Dairay *et al.* (2015), and (A7) simplifies and becomes (2.1), i.e.

$$U_\infty \frac{dA}{dx} = \langle \mathcal{L}(t)(\tilde{V}_n - \tilde{V}_f) \rangle = \mathcal{L} v_n \quad (\text{A } 8)$$

which determines the exact sense in which v_n is an average local propagation velocity:

$$v_n = \langle \int_{\partial \mathcal{A}_t(x)} (V_n - V_f) dl \rangle / \mathcal{L}. \quad (\text{A } 9)$$

To check how well the left hand side of (2.1) approximates the left hand side of (A7) we have used the one saved 3D realisation in our disposal (one time shot) of our DNS flow and have calculated the ratio of $\frac{d}{dx} \int_{\mathcal{A}_t(x)} u dydz$ to $U_\infty \frac{dA_t}{dx}$ for one particular time t but

for all streamwise positions x/L_b between 50 and 100. This instantaneous ratio is within 1 ± 0.05 for the vast majority of values of x/L_b and equals 0.998 when averaged over x .

Whereas (A8) can only be used in turbulent wakes, (A6) and (A7) can also be used in jets which opens an avenue for generalisation of this paper's approach to other turbulent shear flows.

REFERENCES

- ATTILI, A., CRISTANCHO, J. C. & BISETTI, F. 2014 Statistics of the turbulent/non-turbulent interface in a spatially developing mixing layer. *J. Turbul.* **15** (9), 555–568.
- BISSET, D. K., HUNT, J. C. R. & ROGERS, M. M. 2002 The turbulent/non-turbulent interface bounding a far wake. *J. Fluid Mech.* **451**, 383–410.
- BORRELL, G. & JIMÉNEZ, J. 2016 Properties of the turbulent/non-turbulent interface in boundary layers. *J. Fluid Mech.* **801**, 554–596.
- CHAUHAN, K., PHILIP, J., DE SILVA, C. M., HUTCHINS, N. & MARUSIC, I. 2014 The turbulent/non-turbulent interface and entrainment in a boundary layer. *J. Fluid Mech.* **742**, 119–151.
- CORRSIN, S. & KISTLER, A. L. 1955 Free-stream boundaries of turbulent flows. *NACA Tech. Rep.* **1224**, 1033–1064.
- DAIRAY, T., OBLIGADO, M. & VASSILICOS, J. C. 2015 Non-equilibrium scaling laws in axisymmetric turbulent wakes. *J. Fluid Mech.* **781**, 166–195.
- DAIRAY, T. & VASSILICOS, J. C. 2016 Direct numerical simulation of a turbulent wake: The non-equilibrium dissipation law. *Int. J. Heat Fluid Flow* **62**, 68–74.
- GAMPERT, M., KLEINHEINZ, K., PETERS, N. & PITSCHE, H. 2014 Experimental and numerical study of the scalar turbulent/non-turbulent interface layer in a jet flow. *Flow Turbul. Combust.* **92** (1-2), 429–449.
- GEORGE, W. K. 1989 The self-preservation of turbulent flows and its relation to initial conditions and coherent structures. In *Advances in turbulence* (ed. W. K. George & R. Arndt), pp. 39–73. Hemisphere.
- GOTO, S. & VASSILICOS, J. C. 2015 Energy dissipation and flux laws for unsteady turbulence. *Phys. Lett. A* **379** (16), 1144–1148.
- GOTO, S. & VASSILICOS, J. C. 2016a Local equilibrium hypothesis and Taylor's dissipation law. *Fluid Dyn. Res.* **48**, 021402.
- GOTO, S. & VASSILICOS, J. C. 2016b Unsteady turbulence cascades. *Phys. Rev. E* **94** (5), 053108.
- HOLZNER, M. & LÜTHI, B. 2011 Laminar superlayer at the turbulence boundary. *Phys. Rev. Lett.* **106** (13), 134503.
- LARUE, J. C. & LIBBY, P. A. 1976 Statistical properties of the interface in the turbulent wake of a heated cylinder. *Phys. Fluids* **19** (12), 1864–1875.
- MANDELBROT, B. B. 1982 *The Fractal Geometry of Nature*. W. H. Freeman and Company.
- MISTRY, D., PHILIP, J., DAWSON, J. R. & MARUSIC, I. 2016 Entrainment at multi-scales across the turbulent/non-turbulent interface in an axisymmetric jet. *J. Fluid Mech.* **802**, 690–725.
- NEDIĆ, J., VASSILICOS, J. C. & GANAPATHISUBRAMANI, B. 2013 Axisymmetric turbulent wakes with new nonequilibrium similarity scalings. *Phys. Rev. Lett.* **111** (14), 144503.
- OBLIGADO, M., DAIRAY, T. & VASSILICOS, J. C. 2016 Nonequilibrium scalings of turbulent wakes. *Phys. Rev. Fluids* **1** (4), 044409.
- PARNAUDEAU, P., CARLIER, J., HEITZ, D. & LAMBALLAIS, E. 2008 Experimental and numerical studies of the flow over a circular cylinder at reynolds number 3900. *Phys. Fluids* **20** (8), 085101.
- POPE, S. B. 2000 *Turbulent Flows*. Cambridge University Press.
- REDFORD, J. A., CASTRO, I. P. & COLEMAN, G. N. 2012 On the universality of turbulent axisymmetric wakes. *J. Fluid Mech.* **710**, 419–452.
- DA SILVA, C. B., HUNT, J. C. R., EAMES, I. & WESTERWEEL, J. 2014 Interfacial layers between regions of different turbulence intensity. *Annu. Rev. Fluid Mech.* **46**, 567–590.
- SREENIVASAN, K. R., RAMSHANKAR, R. & MENEVEAU, C. H. 1989 Mixing, entrainment and fractal dimensions of surfaces in turbulent flows. *Proc. R. Soc. Lond.* **421**, 79–108.

- TAVEIRA, R. R. & DA SILVA, C. B. 2014 Characteristics of the viscous superlayer in shear free turbulence and in planar turbulent jets. *Phys. Fluids* **26**, 021702.
- TENNEKES, H. & LUMLEY, J. L. 1972 *A First Course in Turbulence*. MIT Press.
- TOWNSEND, A. A. 1976 *The Structure of Turbulent Shear Flow*. Cambridge University Press.
- VALENTE, P. C. & VASSILICOS, J. C. 2012 Universal dissipation scaling for nonequilibrium turbulence. *Phys. Rev. Lett.* **108** (21), 214503.
- VALENTE, P. C. & VASSILICOS, J. C. 2014 The non-equilibrium region of grid-generated decaying turbulence. *J. Fluid Mech.* **744**, 5–37.
- VASSILICOS, J. C. 2015 Dissipation in turbulent flows. *Annu. Rev. Fluid Mech.* **47**, 95–114.
- WATANABE, T., RILEY, J. J., DE BRUYN KOPS, S. M., DIAMESSIS, P. J. & ZHOU, Q. 2016 Turbulent/non-turbulent interfaces in wakes in stably-stratified fluids. *J. Fluid Mech.* **797**, 567–590.
- WATANABE, T., SAKAI, Y., NAGATA, K., ITO, Y. & HAYASE, T. 2014 Enstrophy and passive scalar transport near the turbulent/non-turbulent interface in a turbulent planar jet flow. *Phys. Fluids* **26** (10), 105103.
- WATANABE, T., SAKAI, Y., NAGATA, K., ITO, Y. & HAYASE, T. 2015 Turbulent mixing of passive scalar near turbulent and non-turbulent interface in mixing layers. *Phys. Fluids* **27** (8), 085109.
- WESTERWEEL, J., FUKUSHIMA, C., PEDERSEN, J. M. & HUNT, J. C. R. 2009 Momentum and scalar transport at the turbulent/non-turbulent interface of a jet. *J. Fluid Mech.* **631**, 199–230.